Bioconjugate Chemistry

Article

Cite This: Bioconjugate Chem. 2019, 30, 1658−1664

pubs.acs.org/bc

Surface Coordination of Black Phosphorus with Modified Cisplatin

Jianing Zhang,[†,∥] Yue Ma,[†,∥] Kuan Hu,[†] Yuan Feng,[†] Si Chen,[‡] Xiaoyang Yang,[†] Jacky Fong-Chuen Loo,[§] Han Zhang,[‡] Feng Yin,*[,†] and Zigang Li*[,†]

[†]State Key Laboratory of Chemical Oncogenomics, School of Chemical Biology and Biotechnology, Peking University Shenzhen Graduate School, Shenzhen 518055, China

[‡]SZU-NUS Collaborative Innovation Center for Optoelectronic Science and Technology and Key Laboratory of Optoelectronic Devices and Systems of Ministry of Education and Guangdong Province College of Optoelectronic Engineering, Shenzhen University, Shenzhen 518060, China

[§]Department of Biomedical Engineering, The Chinese University of Hong Kong, Hong Kong, SAR 999077, China

Supporting Information

ABSTRACT: Black phosphorus (BP) is a two-dimensional (2D) nanomaterial with high charge-carrier mobility, a tunable direct bandgap, and a unique in-plane anisotropic structure; however, the easiness of BP oxidation into P_xO_y species in ambient conditions largely limits its applications. In this study, modified cisplatin−Pt−NO_3 [Pt-$(NH_3)_2(NO_3)_2$] is used for surface coordination with BP nanosheets to generate Pt@BP, which maintains the surface morphology and properties of BP nanosheets for more than 24 h in ambient conditions. In addition, Pt@BP interacts with DNA both in vitro and in cell. Pt@BP shows a good cellular uptake rate and significantly increases the drug sensitivity of cisplatin-resistant cancer cell lines (A2780 and HepG2) compared with unmodified cisplatin. Our study is the first attempt to stabilize bare BP with cationic cisplatin species, and the generated Pt@BP could be used for potential synergistic photothermal/chemotherapy of cisplatin-resistant cancer.

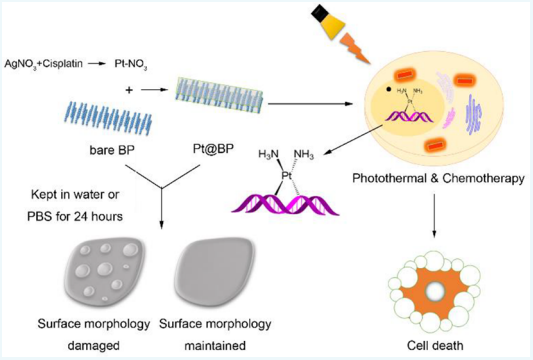

Two-dimensional (2D) materials, such as graphene, hexagonal boron nitride (hBN), and transition metal dichalcogenide (TMD), are of increasing research interest for their large surface-area-to-volume ratio, good electrical conductivity, and easy functionalization.[1−5] As a new member of two-dimensional materials, black phosphorus (BP) possesses anisotropic, electronic, and optical properties[6−8] and has been widely applied in many promising fields and has many potential applications, including photocatalysis,[9−11] semiconductors,[12−17] rechargeable batteries,[18,19] and sensors.[20,21] Phosphorus (P) is one of the most vital elements for all living organisms and acts as a constituent of essential biomolecules and as a major contributor to almost all metabolic processes.[22] When introduced in vivo, BP is of higher biocompatibility and is finally metabolized into nontoxic phosphates and phosphonates in the physiological environment.[23,24] However, BP's instability in ambient conditions is the main hurdle for BP's real applications.[25]

The commonly used methods of black phosphorus modification are effective surface functionalization, including capping layer protection,[26−30] and surface chemical modification, including covalent and noncovalent modification,[31−33] among others. Capping layers have been developed to encapsulate BP and enhance the stability of BP nanosheets, but oxygen and water may enter through the interfaces causing eventual breakdown.[34] Thus, preventing the reaction between BP and oxygen in air and water is crucial to enhance its stability,[35] and a surface coordination strategy could meet this requirement by occupying the lone pair electrons on the surfaces of BP nanosheets with suitable cationic elements or groups.[36] Several cationic ions, including aryl diazonium,[37] titanium sulfonate ligand,[31] Ag^+,[36] 7,7,8,8-tetracyano-*p*-quinodi-methane (TCNQ),[38] and aryl iodonium salts[39] have been used to coordinate with the surfaces of BP nanosheets in order to enhance the nanosheets' stability. However, on the basis of our knowledge, no investigation has utilized a metal complex possessing anticancer activity to coordinate with BP. Cisplatin $[Pt(NH_3)_2Cl_2]$ is one of the most widely used anticancer drugs in treating testicular, head, neck, non-small-cell lung, cervical, and other cancers.[40,41] Toxicity and resistance are the two main drawbacks associated with cisplatin.[42,43] Many reasons have been demonstrated to cause cisplatin resistances; one major reason is the decreased intracellular accumulation of the platinum.[44,45] To address the cellular uptake issue of various cisplatin-resistant cell lines, various nanodelivery systems have been developed and effectively improved the cellular uptake efficiency of cisplatin-resistant cancer cells.[46,47]

Received: February 15, 2019
Revised: April 30, 2019
Published: May 9, 2019

DOI: 10.1021/acs.bioconjchem.9b00128
Bioconjugate Chem. 2019, 30, 1658−1664

Thus, we envisioned Pt as a potentially suitable metal to coordinate with BP. Cisplatin and oxaliplatin were directly reacted with a BP nanosheet, and no coordination was detected. We think increasing the positive valence may be helpful, so the Pt(IV) complex oxidized from cisplatin by H_2O_2 was then tested. However, still no coordination was observed. We think the Pt complexes we used are generally neutral, which may not provide strong enough coordination with BP. Then, we replaced two chloride ions on cisplatin by nitrate ions to better expose the cationic Pt(II). The generated Pt−NO_3 [$Pt(NH_3)_2(NO_3)_2$] reacted smoothly with BP nanosheets to form Pt@BP, which could maintain the surface morphology and properties of BP nanosheets for at least 24 h in ambient conditions. Both Pt−NO_3 and Pt@BP could react with 5′-GMP and single strand DNAs as cisplatin does. Pt@BP showed better cell cytotoxicity for cisplatin-resistant cell lines (HepG2-R and A2780-R) and maintained the photothermal effect of BP after exposure under ambient conditions for over 24 h. This study is the first attempt to coordinate Pt(II) with a bare BP nanosheet for potential biomedicine application.

RESULTS AND DISCUSSION

The BP nanosheets were synthesized in *N*-methyl-2-pyrrolidone (NMP) by a liquid exfoliation technique.[31] We first used cisplatin, oxaliplatin, and Pt(IV) oxidized from cisplatin by H_2O_2 to respectively react with bare BP. No obvious changes of binding energy were detected by high-resolution X-ray photoelectron spectroscopy (HR-XPS), indicating there were no coordination between cisplatin/oxaliplatin/Pt(IV) and bare BP (Figure S1). To further expose the cationic core of the Pt complex, we replaced two chloride ions of cisplatin with nitrates to further improve the electropositivity of cisplatin. Pt−NO_3 [$Pt(NH_3)_2(NO_3)_2$] was prepared by letting cisplatin react with 2 equiv of $AgNO_3$ in water for 12 h as previously reported[48] (Figure 1A).

According to the HR-XPS results in Figures S1 and S2, both cisplatin and Pt−NO_3 showed representative peaks of divalent platinum ions, Pt 4f 7/2 and Pt 4f 5/2, with binding energies of at 72.8 eV (cisplatin)/73.0 eV (Pt−NO_3) and 76.1 eV (cisplatin) /76.4 eV (Pt−NO_3), respectively. The results of Fourier transform infrared spectroscopy (FT-IR) in Figure S3 indicated that the Pt−NO_3 has successfully touched to the surface of bare BP, with the characteristic peaks of Pt−NO_3 (2920, 2852 cm^{-1}). Then, bare BP nanosheets were reacted with Pt−NO_3 in NMP/water at room temperature in the protection of nitrogen for 18 h to generate Pt@BP. Both Pt@BP and bare BP showed three prominent Raman peaks; the three peaks of Pt@BP were at 356.8, 433.1, and 459.8 cm^{-1}, red-shifted from the three main peaks of BP by about 7.1, 8.8, and 8.9 cm^{-1}, respectively (Figure 1B). When Pt−NO_3 interacted with bare BP, the oscillation of the P atoms was weakened, which reduced the Raman scattering energy and resulted in the red-shifts of these three Raman peaks of Pt@BP. HR-XPS was then utilized to analyze the detailed chemical composition and the bonding configuration of phosphorus atoms of Pt@BP and bare BP. As shown in Figure 1C, in the P 2p spectrum, the bare BP showed the characteristic P 2p 3/2 and P 2p 1/2 doublet of crystalline BP at 129.9 and 130.7 eV, respectively.[49] In addition, intense oxidized phosphorus (P_xO_y) sub-bands emerged at 134.0 eV as a result of partial oxidation. This binding energy of oxidized BP has been observed from bare BP by XPS previously.[50] In our case, the binding energy of Pt@BP was detected at 133.0 eV, which was in agreement with

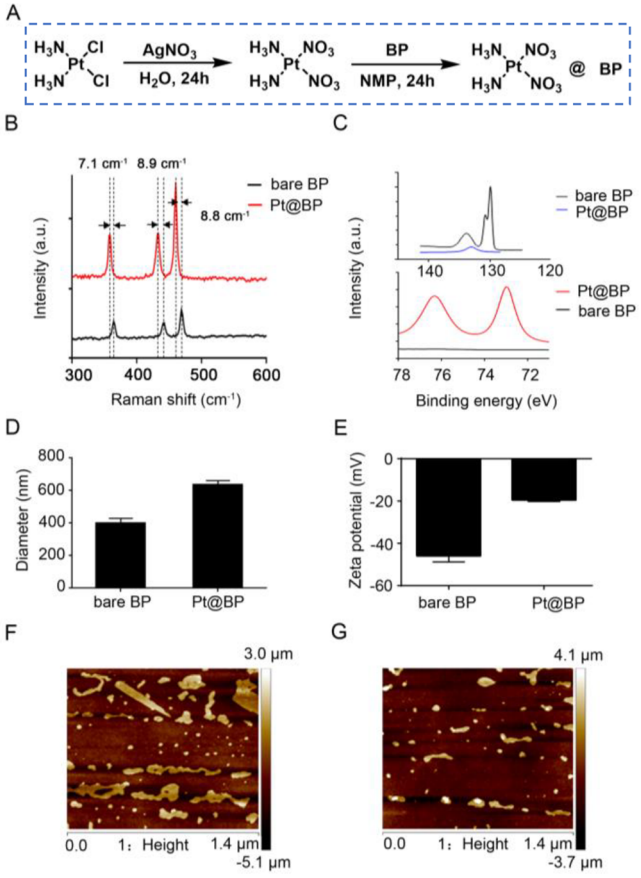

Figure 1. Fabrication and characterization of Pt@BP. (A) Preparation of Pt@BP; (B) Raman spectra of bare BP and Pt@BP tested on the mica sheets; (C) HR-XPS spectra of P 2p (up) and Pt 4f (down) tested on the Si/SiO_2 substrates; (D) hydrodynamic size analysis of bare BP and Pt@BP; (E) zeta potential of bare BP and Pt@BP. AFM images of the bare BP (F) and Pt@BP (G) tested on the Si/SiO_2 substrates.

the binding energy of metal-ion-coordinated BP.[31,36] The distinguishable higher binding energy of Pt@BP could be caused by the coordination between the lone pair electrons of bare BP and the empty orbital of the platinum. These sub-bands were attributed to the formation of phosphorus−platinum covalent bonds. In the Pt 4f spectrum, the peaks at binding energies of 73.0 and 76.3 eV in Pt@BP were ascribed to the bivalent platinum ion, but the bare BP showed no obvious binding energy in the Pt 4f spectrum. All the XPS results indicated the successful interaction of Pt−NO_3 and BP nanosheets. After the successful interaction, the average size of Pt@BP was about 635.5 nm (Figure 1D), and the zeta potential of Pt@BP raised from −44.33 to −22.33 mV (Figure 1E).

As shown in Figure 1F, the atomic force microscopy (AFM) images showed Pt@BP had better dispensability and smaller size than bare BP. These results demonstrated that the Pt−NO_3 could interact with BP nanosheets covalently and enhance the dispensability.

Then, we assessed the releasing percentage of Pt−NO_3 from the Pt@BP nanocomplex in different conditions, including 1× PBS (pH 7.4), DMEM, thermal heat in DMEM, 5× PBS (pH 7.4), 10 mM GSH in 1× PBS (pH 7.4), 1× PBS (pH 6.0), and 10 mM GSH in 1× PBS (pH 6.0) as shown in Figure S5. And we found only 14% of the Pt−NO_3 was released over 10 days

DOI: 10.1021/acs.bioconjchem.9b00128
Bioconjugate Chem. 2019, 30, 1658−1664

in 1× PBS (pH 7.4), and 10% of the Pt−NO_3 was released over 48 h in cell culture medium (DMEM), suggesting the binding between Pt−NO_3 and BP was relatively stable in normal physiological and extracellular cell culture medium. Further, only 9% of the Pt−NO_3 was released under the NIR treatment over 60 min, while conventional photothermal therapy resulted in less than 10 min, suggesting this binding was fairly stable in the photothermal condition. However, 33% of the Pt−NO_3 was released over 48 h in 5× PBS, and 45% of Pt−NO_3 was released over 48 h in 10 mM GSH, suggesting the high salt concentration and GSH have significant affects to the coordination between Pt−NO_3 and BP nanosheets. When the pH of 1× PBS solution reduced from 7.4 to 6.0, the Pt−NO_3 releasing percentage increased from 14 to 45% following the change of pH. As most cancer cells have a lower pH of about 6.0 with excessive GSH,[51] which is different from normal cells, we further simulated the tumor cells' intracellular environment and found the releasing percentage increased drastically from 45 to 79% after the pH of PBS solution became 6.0 with 10 mM GSH. These results indicate that the release of Pt−NO_3 from the Pt@BP nanocomplex is a condition dependent process, which is important for the treatment of neoplasms. And this is also in accord with the cytotoxicity experiments for both normal cells and cancer cells described below.

To evaluate the role of Pt−NO_3 coordination to the photothermal performance of BP nanosheets, the solution temperature as a function of time was studied by using the 808 nm NIR laser (1.0 Wc^{-2} at power density) as the light source (Figure S4). The solution temperature of both bare BP and Pt@BP increased by 16 °C after irradiation for 20 min, suggesting there are no obvious differences between the photothermal performance before and after the Pt−NO_3 coordination.

Then, we assessed the stabilization effect of Pt−NO_3 modification (Figure 2). The samples were then divided into three groups; the first group was kept in the N_2 glovebox for 24 h (Figure S7), while the second or third group was kept at ambient conditions in water and PBS, respectively, for 24 h (Figure 2A). The surface of bare BP appeared to be smooth at initial exposure time (0 h) both in the N_2 glovebox and air, and the surrounding Si/SiO_2 substrate was featureless in the SEM micrograph. After exposure in water and PBS for 24 h, the surface of bare BP became rough. This might be caused by the formation of water droplets on the surface of the sheets. Then, P was oxidized and hydrated into final PO_4^{3-} anions.[49] The surface morphology of BP nanosheets was damaged. These results are consistent with the previously reported morphological changes on BP sheets in air.[50] In contrast, there were no obvious surface morphology changes of Pt@BP when it was exposed both in water and PBS after 24 h. Then, the stability of BP and Pt@BP was further examined for a longer duration of time as shown in Figure 2B. After 10 days in ambient conditions, bare BP had completely lost its surface morphology, while Pt@BP showed no obvious changes. All these results provided direct evidence of Pt−NO_3's protective effects of BP.

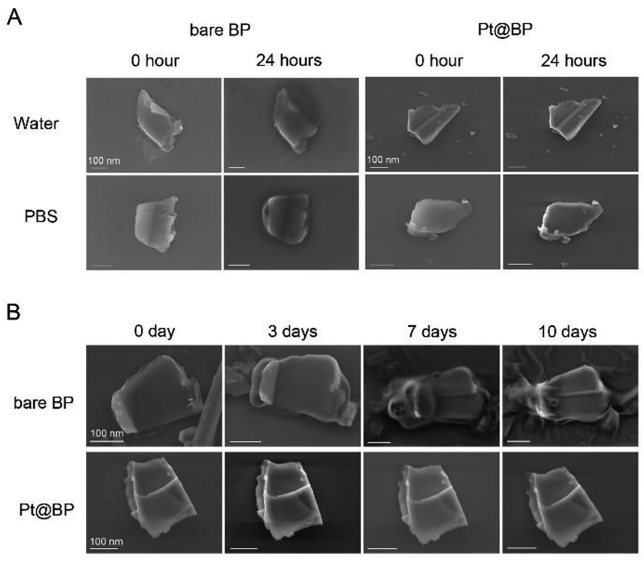

Figure 2. SEM images of bare BP and Pt@BP exposed in water and PBS for (A) 0 and 24 h or for (B) 0, 3, 7, and 10 days.

The Pt^{II} species is known to interact with nucleophiles and form stable adducts such as Pt−DNA covalent cross-links.[39,40] It was documented that platinum(II) could bind to the N7 position of GMP to form stable Pt−GMP adducts, showing a downfield shift of the H8 proton (δ = 8.1 ppm) in the ^{1}H NMR spectrum.[52] Pt−NO_3 and Pt@BP were then treated with an excess of guanosine monophosphate (5′-GMP, 1:2 ratio in D_2O). As shown in Figure 3A, after 5 h of reaction, new peaks of the H8 proton appeared at δ = 8.67 and 8.51 ppm for the reaction products of Pt−NO_3 and Pt@BP with 5′-GMP, respectively. These results clearly indicated that both Pt−NO_3 and Pt@BP could effectively bind to the N7 position of GMP.

The reaction of cisplatin and DNA would cause the interstrand and intrastrand cross-linking of DNA.[39] We first detected whether Pt−NO_3 and Pt@BP could bind to DNA in vitro and cause the cross-links of DNA. AFM has been used for Pt−DNA interaction, and cisplatin could lead to an obvious cross-link and aggregation of DNA. In our experiments, we detected that Pt−NO_3 and Pt@BP could bind to DNA and cause the ssDNA cross-links (Figure 3B−D). The sequence of the used ssDNA is shown in Table S1.

These results are in good agreement with the previously reported cross-linking and aggregation of DNA treated by cisplatin observed in the AFM images.[53] We also tested whether Pt−NO_3 and Pt@BP could competitively bind to DNA in vitro. Acridine Orange (AO), a standard DNA intercalator, exhibits strong emission at about 525 nm (λ excitation = 490 nm) in aqueous solutions when it randomly binds with the outside phosphate groups of dsDNAs.[52] In a binding competition assay, the emission intensity of AO gradually decreased wit an increased amount of Pt−NO_3 or Pt@BP, suggesting the formation of Pt−DNA adducts (Figure 3E,F) (sequence of used dsDNA shown in Table S2). All assays supported that both Pt−NO_3 and Pt@BP could interact with DNA and cause DNA cross-links in vitro.

The levels of bioavailable Pt(II) of cisplatin-, Pt−NO_3-, and Pt@BP-treated cells were then analyzed by ICP-MS. Four cell lines, cisplatin-resistant HepG2-R and A2780-R cells and cisplatin-sensitive HepG2-N and A2780-N cells, were treated with 15 ppm of cisplatin, Pt−NO_3, and Pt@BP at 37 °C for 12 h. The total DNA of treated cells was then purified for subsequent ICP-MS analysis. Our data showed that (Figures 3G,H and S8) Pt−NO_3-treated cells had the highest level of DNA-bound Pt, followed by 808 nm laser-treated Pt@BP and then Pt@BP, while cisplatin-treated cells contained the minimum amount of DNA-bound Pt, suggesting the lowest

DOI: 10.1021/acs.bioconjchem.9b00128
Bioconjugate Chem. 2019, 30, 1658−1664

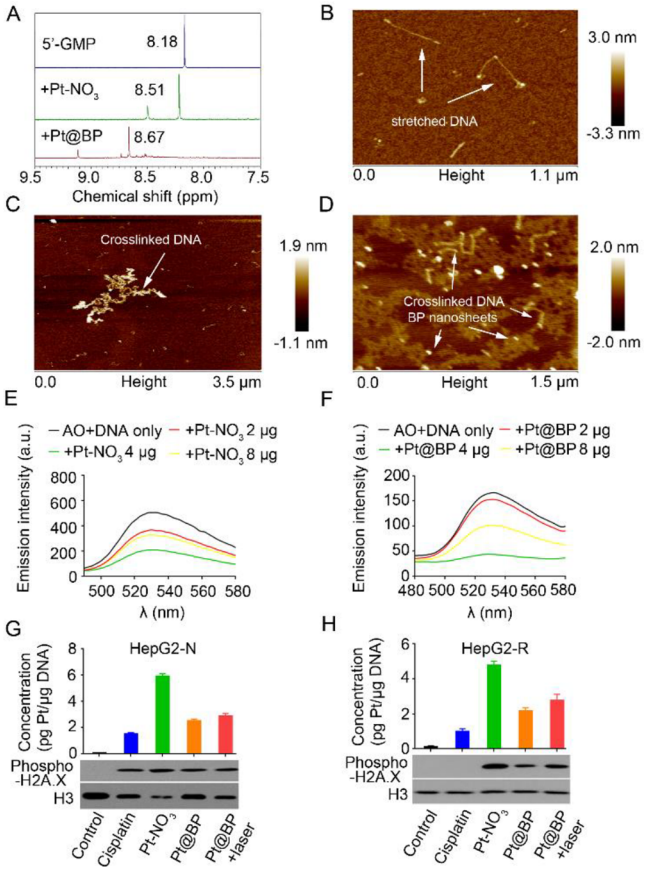

Figure 3. Pt−NO_3 and Pt@BP could react with DNA in vitro and in vivo. (A) ^{1}H NMR spectra of 5′-GMP only (up), Pt−NO_3 (middle), and Pt@BP (bottom) in the presence of 5′-GMP recorded in D_2O; AFM images of (B) stretched ssDNA, (C) ssDNA in the presence of Pt−NO_3, and (D) Pt@BP for 1 h of incubation, respectively; emission spectra of AO in the presence of dsDNA and (E) Pt−NO_3 or (F) Pt@BP under different doses. Pt−NO_3/Pt@BP, DNA (120 μM), and AO (20 μM) were incubated in 5% DMSO/ddH_2O medium to confirm the reaction of Pt−NO_3/Pt@BP and DNA. DNA-bound Pt in (G) HepG2-N and (H) HepG2-R cell lines was treated with cisplatin, Pt−NO_3, and Pt@BP nanoparticles (10 ppm) for 12 h and the corresponding phosphorylated H2A.X level in cells.

cellular uptake level of cisplatin. These results suggested that Pt−NO_3 and Pt@BP have better cellular uptake and bioavailability than unmodified cisplatin in both cisplatin-sensitive cell lines and cisplatin-resistant cell lines.

Phosphorylation of H2A.X is a sensitive marker of cisplatin induced DNA damage.[54] The phosphorylation levels of H2A.X in HepG2-R and HepG2-N (Figure 3G,H), A2780-R and A2780-N cell lines (Figure S8) treated with cisplatin, Pt−NO_3, and Pt@BP (10 ppm) for 12 h were analyzed, and the expression level of phosphorylated H2A.X was significantly higher in Pt@BP-treated cisplatin-resistant cell lines than that in cisplatin-treated cells, which was consistent with the level of Pt−DNA adduct formation detected by ICP-MS. These results demonstrated that Pt@BP could induce a higher level of DNA damage compared with that induced by the same concentration of cisplatin, and these results were in accordance with the previously reported DNA damage induced phosphorylation of H2A.X.[54]

Then, we further tested the cytotoxicity of Pt−NO_3 and Pt@BP. When compared with cisplatin, Pt@BP had lower cytotoxicity for normal cell lines (293T and Chang liver cell lines), although it showed higher cytotoxicity toward cancer cell lines including HeLa, A172, and T47D cells as shown in Figure S9. We further examined the cytotoxicity of Pt, Pt−NO_3, and Pt@BP on cisplatin-sensitive cell lines (HepG2-N and A2780-N) and cisplatin-resistant cell lines (HepG2-R and A2780-R) and found that Pt−NO_3 and Pt@BP have remarkably higher cytotoxicity toward these four cell lines, especially to the cisplatin-resistant HepG2-R (Figure 4B) and A2780-R (Figure S10) cell lines when compared with cisplatin. It is worth noting that Pt−NO_3 showed serious toxicity for all cell lines; thus, it could not be utilized in vivo separately unless combined with other materials, which could effectually reduce the toxicity of Pt−NO_3. In summary, the coordination of Pt−NO_3 to BP nanosheets could effectively reduce the cytotoxicity of Pt−NO_3 and cisplatin for normal cells and significantly increase the cytotoxicity for cisplatin-resistant cell lines.

BP is a highly efficient photosensitizer that can convert NIR light into heat and inhibit the rapid growth of cancer cells. Because of its unique characteristics, BP has been widely used in photodynamic treatment (PDT) and photothermal treatment (PTT).[55] Thus, we further explored the photothermal effect of Pt@BP on HepG2-R (Figure 4C,D) and A2780-R (Figure S11) cell lines. After treatment with a 808 nm near-infrared laser for 10 min, 20 ppm of Pt@BP showed a higher cell inhibition rate for HepG2-R and A2780-R cells compared with bare BP or Pt@BP without NIR treatment. After bare BP and Pt@BP were exposed in humid conditions for 24 h, the cell inhibition rate of bare BP was significantly decreased; however, the cell inhibition rate of NIR-treated Pt@BP had no remarkable changes when compared with freshly prepared Pt@BP. Combining all the experimental evidence, we concluded that Pt−NO_3 functionalization could increase the stability and maintain the PTT properties of bare BP nanosheets under ambient conditions for at least 24 h.

To further investigate the death of cancer cells caused by Pt@BP, a cell apoptosis assay was further performed on HepG2-N/R (Figures 4E,F and S12) and A2780-N/R cell lines (Figure S13). We found that 15 ppm of cisplatin could significantly induce the apoptosis of HepG2-N cells (Figure 4E) and A2780-N cell lines (Figure S13A,B), while it had few apoptosis-promoting effects on HepG2-R (Figure 4F) or A2780-R (Figure S13C,D) cell lines. However, the same concentration of Pt@BP could prominently promote apoptosis of A2780-R and HepG2-R cell lines. When combined with 808 nm light treatment, Pt@BP could cause a remarkable increase of the apoptosis rate in HepG2-R cells and A2789-R cells. In conclusion, Pt@BP could effectively induce the apoptosis of cisplatin-resistant cell lines (HepG2-R and A2780-R), which might be a good strategy for the treatment of cisplatin-resistant tumors.

CONCLUSION

In summary, for the first time, we used the derivative of cisplatin (Pt−NO_3) to modify BP nanosheets, which could stabilize BP nanosheets and show significantly higher anticancer efficacy for cisplatin-resistant cell lines. After Pt−NO_3 modification, BP showed increased surface zeta potential, more suitable sizes, better dispensability, and higher stability in ambient conditions for long duration (10 days). Both Pt−NO_3 and Pt@BP could react with DNA in vitro and cause the intra/interstrand cross-link of DNA as previously reported. In addition, the Pt−NO_3 and Pt@BP showed significantly

DOI: 10.1021/acs.bioconjchem.9b00128
Bioconjugate Chem. 2019, 30, 1658−1664

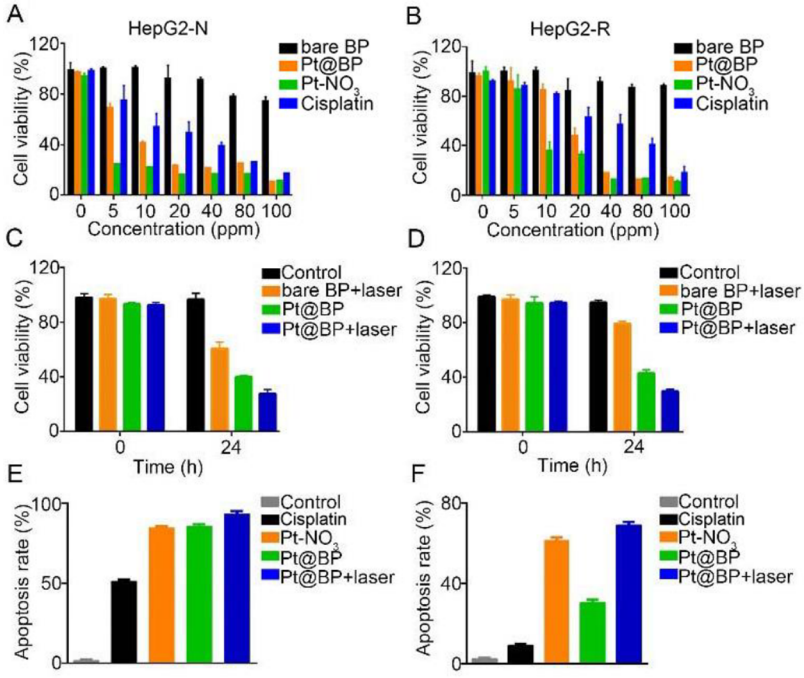

Figure 4. Cell viability assay and cell apoptosis assay of Pt@BP and Pt@BP+laser. The effects of different concentrations of bare BP, Pt@BP, Pt−NO_3, and cisplatin on the growth of (A) HepG2-N and (B) HepG2-R cell lines; PTT effects of 20 ppm of bare BP and Pt@BP for HepG2-R cell lines after exposure in ambient conditions for (C) 0 and (D) 24 h. Pt@BP, Pt−NO_3, and Pt@BP+laser efficiently induce the apoptosis in (E) HepG2-N cells and (F) HepG2-R cells. Cell were stained with Annexin V/PI, and the number of apoptotic cells was measured by flow cytometry. Then, apoptotic cells were counted in the lower right (Q2) and upper right (Q3) for HepG2-N cell lines (Figure S12A,B) and HepG2-R cell lines (Figure S12C,D). The apoptotic cells of each analysis were calculated and normalized to blank. Error bars represent the standard error of mean from three independent experiments.

increased cytotoxicity and apoptotic-promoting capability to the cisplatin-resistant cell lines when compared with cisplatin. Although Pt−NO_3 could also remarkably induce apoptosis in A2780-R and HepG2-R cells, it shows obvious toxicity for all cell lines we used in this study. In addition, after being exposed for 24 h under ambient conditions, NIR-treated Pt@BP could maintain the inhibition rate for HepG2-R and A2780-R cells, while the inhibition rate of bare BP significantly decreased, indicating that the coordination of BP with Pt−NO_3 could maintain the stability and PTT performance of BP nanosheets. In conclusion, we developed a novel strategy for BP modification by the derivative of cisplatin (Pt−NO_3), which could maintain the stabilization and optical properties of BP and assist in cisplatin's cellular accumulation. Pt@BP showed better stability in the medium without noticeable aggregation, conditional dependent release of Pt(II) species, and good synergistic photothermal/chemotherapy. These experimental observations indicated that it may be considered for further in vivo applications.

■ ASSOCIATED CONTENT

Supporting Information

The Supporting Information is available free of charge on the ACS Publications website at DOI: 10.1021/acs.bioconjchem.9b00128.

Additional details on materials and methods. Figures showing HR-XPS spectra, SEM images, cell viability, Western blot, and apoptosis experimental results. Tables showing ssDNA and dsDNA sequences (PDF)

■ AUTHOR INFORMATION

Corresponding Authors

*E-mail: yinfeng@pkusz.edu.cn. (F.Y.)
*E-mail: lizg@pkusz.edu.cn. (Z.L.)

ORCID

Han Zhang: 0000-0002-2197-7270
Zigang Li: 0000-0002-3630-8520

Author Contributions

‖J.Z. and Y.M. contributed equally to this work.

Notes

The authors declare no competing financial interest.

■ ACKNOWLEDGMENTS

We acknowledge financial support from the Natural Science Foundation of China grants 21778009 and 81701818 and from the Shenzhen Science and Technology Innovation Committee, JCYJ20170807144449135, JCYJ20170412150609690, and KQJSCX20170728101942700. This work is supported by the High-Performance Computing Platform of Peking University.

■ REFERENCES

(1) Yin, F., Hu, K., Chen, Y., Yu, M., Wang, D., Wang, Q., Yong, K., Lu, F., Liang, Y., and Li, Z. (2017) SiRNA Delivery with PEGylated Graphene Oxide Nanosheets for Combined Photothermal and Genetherapy for Pancreatic Cancer. *Theranostics 7*, 1133−1148.

(2) Li, Y., Duerloo, K., Wauson, K., and Reed, E. (2016) Structural semiconductor-to-semimetal phase transition in two-dimensional materials induced by electrostatic gating. *Nat. Commun. 7*, 10671.

(3) Georgiou, T., Jalil, R., Belle, B., Britnell, L., Gorbachev, R., Morozov, S., Kim, Y., Gholinia, A., Haigh, S., Makarovsky, O., et al. (2013) Vertical field-effect transistor based on graphene-WS2

DOI: 10.1021/acs.bioconjchem.9b00128
Bioconjugate Chem. 2019, 30, 1658−1664

heterostructures for flexible and transparent electronics. *Nat. Nanotechnol. 8*, 100−103.
(4) Peng, Q., Dearden, A., Crean, J., Han, L., Liu, S., Wen, X., and De, S. (2014) New materials graphyne, graphdiyne, graphone, and graphane: review of properties, synthesis, and application in nanotechnology. *Nanotechnol., Sci. Appl. 7*, 1−29.
(5) Qiu, M., Sun, Z., Sang, D., Han, X., Zhang, H., and Niu, C. (2017) Current progress in black phosphorus materials and their applications in electrochemical energy storage. *Nanoscale 9*, 13384−13403.
(6) Gaharwar, A., Peppas, N., and Khademhosseini, A. (2014) Nanocomposite hydrogels for biomedical applications. *Biotechnol. Bioeng. 111*, 441−453.
(7) Bridgman, P. (1914) Two new modifications of phosphorus. *J. Am. Chem. Soc. 36*, 1344−1363.
(8) Cai, Y., Zhang, G., and Zhang, Y. (2015) Electronic properties of phosphorene/graphene and phosphorene/hexagonal boron nitride heterostructures. *J. Phys. Chem. C 119*, 13929−13936.
(9) Liu, H., Du, Y., Deng, Y., and Ye, P. (2015) Semiconducting black phosphorus: synthesis, transport properties and electronic applications. *Chem. Soc. Rev. 44*, 2732−2743.
(10) Wang, F., Ng, W., Yu, J., Zhu, H., Li, C., Zhang, L., Liu, Z., and Li, Q. (2012) Red phosphorus: an elemental photocatalyst for hydrogen formation from water. *Appl. Catal., B 111*, 409−414.
(11) Shen, Z., Hu, Z., Wang, W., Lee, S., Chan, D., Li, Y., Gu, T., and Yu, J. (2014) Crystalline phosphorus fibers: controllable synthesis and visible-light-driven photocatalytic activity. *Nanoscale 6*, 14163−14167.
(12) Wang, H., Yang, X., Shao, W., Chen, S., Xie, J., Zhang, X., Wang, J., and Xie, Y. (2015) Ultrathin black phosphorus nanosheets for efficient singlet oxygen generation. *J. Am. Chem. Soc. 137*, 11376−11382.
(13) Kou, L., Frauenheim, T., and Chen, C. (2014) Phosphorene as a Superior Gas Sensor: Selective Adsorption and Distinct *I-V* Response. *J. Phys. Chem. Lett. 5*, 2675−2681.
(14) Das, S., Zhang, W., Demarteau, M., Hoffmann, A., Dubey, M., and Roelofs, A. (2014) Tunable transport gap in phosphorene. *Nano Lett. 14*, 5733−5739.
(15) Qiao, J., Kong, X., Hu, Z., Yang, F., and Ji, W. (2014) High-mobility transport anisotropy and linear dichroism in few-layer black phosphorus. *Nat. Commun. 5*, 4475.
(16) Xia, F., Wang, H., and Jia, Y. (2014) Rediscovering black phosphorus as an anisotropic layered material for optoelectronics and electronics. *Nat. Commun. 5*, 4458.
(17) Tran, V., Soklaski, R., Liang, Y., and Yang, L. (2014) Layer-controlled band gap and anisotropic excitons in few-layer black phosphorus. *Phys. Rev. B: Condens. Matter Mater. Phys. 89*, 235319.
(18) Li, L., Yu, Y., Ye, G., Ge, Q., Ou, X., Wu, H., Feng, D., Chen, X., and Zhang, Y. (2014) Black phosphorus field-effect transistors. *Nat. Nanotechnol. 9*, 372−377.
(19) Zhang, H. (2015) Ultrathin two-dimensional nanomaterials. *ACS Nano 9*, 9451−9469.
(20) Zhou, Y., Zhang, M., Guo, Z., Miao, L., Han, S., Wang, Z., Zhang, Z., Zhang, H., and Peng, Z. (2017) Recent advances in black phosphorus-based photonics, electronics, sensors and energy devices. *Mater. Horiz. 4*, 997−1019.
(21) Chen, P., Li, N., Chen, X., Ong, W., and Zhao, X. (2018) The rising star of 2D black phosphorus beyond graphene: synthesis, properties and electronic applications. *2D Mater. 5*, 014002.
(22) Yin, F., Hu, K., Chen, S., Wang, D., Zhang, J., Xie, M., Yang, D., Qiu, M., Zhang, H., and Li, Z. (2017) Black phosphorus quantum dot based novel siRNA delivery systems in human pluripotent teratoma PA-1 cells. *J. Mater. Chem. B 5*, 5433.
(23) Gusmão, R., Sofer, Z., and Pumera, M. (2017) Black Phosphorus Rediscovered: From Bulk Material to Monolayers. *Angew. Chem., Int. Ed. 56*, 8052−8072.
(24) Ling, X., Wang, H., Huang, S., Xia, F., and Dresselhaus, M. (2015) The renaissance of black phosphorus. *Proc. Natl. Acad. Sci. U. S. A. 112*, 4523.
(25) Zhang, X., Xie, H., Liu, Z., Tan, C., Luo, Z., Li, H., Li, H., Lin, J., Sun, L., Chen, W., et al. (2015) Black phosphorus quantum dots. *Angew. Chem., Int. Ed. 54*, 3653.
(26) Wood, J., Wells, S., Jariwala, D., Chen, K., Cho, E., Sangwan, V., Liu, X., Lauhon, L., Marks, T., and Hersam, M. C. (2014) Effective passivation of exfoliated black phosphorus transistors against ambient degradation. *Nano Lett. 14*, 6964−6970.
(27) Kim, J., Liu, Y., Zhu, W., Kim, S., Wu, D., Tao, L., Dodabalapur, A., Lai, K., and Akinwande, D. (2015) Toward air-stable multilayer phosphorene thin-films and transistors. *Sci. Rep. 5*, 8989.
(28) Uk Lee, H., Lee, S., Won, J., Son, B., Choi, S., Kim, Y., Park, S., Kim, H., Lee, Y., and Lee, J. (2015) Stable semiconductor black phosphorus (BP)@ titanium dioxide (TiO_2) hybrid photocatalysts. *Sci. Rep. 5*, 8691.
(29) Li, P., Zhang, D., Liu, J., Chang, H., Sun, Y., and Yin, N. (2015) Air-stable black phosphorus devices for ion sensing. *ACS Appl. Mater. Interfaces 7*, 24396−24402.
(30) Shao, J., Xie, H., Huang, H., Li, Z., Sun, Z., Xu, Y., Xiao, Q., Yu, X., Zhao, Y., Zhang, H., et al. (2016) Biodegradable black phosphorus-based nanospheres for in vivo photothermal cancer therapy. *Nat. Commun. 7*, 12967.
(31) Zhao, Y., Wang, H., Huang, H., Xiao, Q., Xu, Y., Guo, Z., Xie, H., Shao, J., Sun, Z., Han, W., et al. (2016) Surface coordination of black phosphorus for robust air and water stability. *Angew. Chem., Int. Ed. 55*, 5003−5007.
(32) Ryder, C., Wood, J., Wells, S., Yang, Y., Jariwala, D., Marks, T., Schatz, G., and Hersam, M. (2016) Covalent functionalization and passivation of exfoliated black phosphorus via aryl diazonium chemistry. *Nat. Chem. 8*, 597−602.
(33) Li, P., Zhang, D., Liu, J., Chang, H., Sun, Y., and Yin, N. (2015) Air-stable black phosphorus devices for ion sensing. *ACS Appl. Mater. Interfaces 7*, 24396−24402.
(34) Island, J. O., Steele, G. A., van der Zant, H. S. J., and Castellanos-Gomez, A. (2015) Environmental instability of few-layer black phosphorus. *2D Mater. 2*, 011002.
(35) Favron, A., Gaufrès, E., Fossard, F., Phaneuf-L'Heureux, A., Tang, N., Lévesque, P., Loiseau, A., Leonelli, R., Francoeur, S., and Martel, R. (2015) Photooxidation and quantum confinement effects in exfoliated black phosphorus. *Nat. Mater. 14*, 826.
(36) Guo, Z., Chen, S., Wang, Z., Yang, Z., Liu, F., Xu, Y., Wang, J., Yi, Y., Zhang, H., Liao, L., et al. (2017) Metal-Ion-Modified Black Phosphorus with Enhanced Stability and Transistor Performance. *Adv. Mater. 29*, 1703811.
(37) Abate, Y., Akinwande, D., Gamage, S., Wang, H., Snure, M., Poudel, N., and Cronin, S. (2018) Recent Progress on Stability and Passivation of Black Phosphorus. *Adv. Mater. 30*, 1704749.
(38) Abellán, G., Lloret, V., Mundloch, U., Marcia, M., Neiss, C., Görling, A., Varela, M., Hauke, F., and Hirsch, A. (2016) Noncovalent functionalization of black phosphorus. *Angew. Chem., Int. Ed. 55*, 14557−14562.
(39) van Druenen, M., Davitt, F., Collins, T., Glynn, C., O'Dwyer, C., Holmes, J., and Collins, G. (2018) Covalent Functionalization of Few-Layer Black Phosphorus using Iodonium Salts and Comparison to Diazonium Modified Black Phosphorus. *Chem. Mater. 30*, 4667−4674.
(40) Malinge, J., Giraud-Panis, M., and Leng, M. (1999) Interstrand cross-links of cisplatin induce striking distortions in DNA. *J. Inorg. Biochem. 77*, 23−29.
(41) Kelland, L. (2007) The resurgence of platinum-based cancer chemotherapy. *Nat. Rev. Cancer 7*, 573−584.
(42) Bancroft, D., Lepre, C., and Lippard, S. (1990) Platinum-195 NMR kinetic and mechanistic studies of cis-and trans-diamminedichloroplatinum (II) binding to DNA. *J. Am. Chem. Soc. 112*, 6860−6871.
(43) Stordal, B., and Davey, M. (2007) Understanding cisplatin resistance using cellular models. *IUBMB Life 59*, 696−699.
(44) Beretta, G., Gatti, L., Tinelli, S., Corna, E., Colangelo, D., Zunino, F., and Perego, P. (2004) Cellular pharmacology of cisplatin in relation to the expression of human copper transporter CTR1 in

DOI: 10.1021/acs.bioconjchem.9b00128
Bioconjugate Chem. 2019, 30, 1658−1664

different pairs of cisplatin-sensitive and-resistant cells. *Biochem. Pharmacol. 68*, 283−291.
(45) Galluzzi, L., Senovilla, L., Vitale, I., Michels, J., Martins, I., Kepp, O., Castedo, M., and Kroemer, G. (2012) Molecular mechanisms of cisplatin resistance. *Oncogene 31*, 1869−1883.
(46) Ishida, S., Lee, J., Thiele, D., and Herskowitz, I. (2002) Uptake of the anticancer drug cisplatin mediated by the copper transporter Ctr1 in yeast and mammals. *Proc. Natl. Acad. Sci. U. S. A. 99*, 14298−14302.
(47) Min, Y., Mao, C., Chen, S., Ma, G., Wang, J., and Liu, Y. (2012) Combating the drug resistance of cisplatin using a platinum prodrug based delivery system. *Angew. Chem., Int. Ed. 51*, 6742−6747.
(48) Yang, X., Du, X., Liu, Y., Zhu, Y., Liu, Y., Li, Y., and Wang, J. (2014) Rational design of polyion complex nanoparticles to overcome cisplatin resistance in cancer therapy. *Adv. Mater. 26*, 931−936.
(49) Sun, Z., Xie, H., Tang, S., Yu, X., Guo, Z., Shao, J., Zhang, H., Huang, H., Wang, H., and Chu, P. (2015) Ultrasmall black phosphorus quantum dots: synthesis and use as photothermal agents. *Angew. Chem. 127*, 11688−11692.
(50) Zhang, J., Chen, S., Ma, Y., Wang, D., Zhang, J., Wang, Y., Li, W., Yu, Z., Zhang, H., Yin, F., et al. (2018) Organosilicon modification enhanced the stability of black phosphorus nanosheets at ambient conditions. *J. Mater. Chem. B 6*, 4065.
(51) Bansal, A., and Simon, M. C. (2018) Glutathione metabolism in cancer progression and treatment resistance. *J. Cell Biol. 217*, 2291−2298.
(52) Sakoda, M., Hiromi, K., and Akasaka, K. (1971) Kinetic studies of interaction between acridine orange and DNA. *Biopolymers 10*, 1003−1012.
(53) Hou, X., Zhang, X., Wei, K., Ji, C., Dou, S., Wang, W., Li, M., and Wang, P. (2009) Cisplatin induces loop structures and condensation of single DNA molecules. *Nucleic Acids Res. 37*, 1400−1410.
(54) Clingen, P., Wu, J., Miller, J., Mistry, N., Chin, F., Wynne, P., Prise, K., and Hartley, J. A. (2008) Histone H2AX phosphorylation as a molecular pharmacological marker for DNA interstrand crosslink cancer chemotherapy. *Biochem. Pharmacol. 76*, 19−27.
(55) Chen, W., Ouyang, J., Liu, H., Chen, M., Zeng, K., Sheng, J., Liu, Z., Han, Y., Wang, L., and Li, J. (2017) Black Phosphorus Nanosheet-Based Drug Delivery System for Synergistic Photodynamic/ Photothermal/Chemotherapy of Cancer. *Adv. Mater. 29*, 1603864.

DOI: 10.1021/acs.bioconjchem.9b00128
Bioconjugate Chem. 2019, 30, 1658−1664